



Radio Science®

RESEARCH ARTICLE

10.1029/2022RS007634

Key Points:

- Using the JME radar data to study the diurnal, seasonal, and Kp dependencies of mid-latitude F-region scattering occurrence rate
- At night, there is a long and narrow area with an increasing scattering occurrence rate in the mid-latitude
- Gradient drift instability may influence the distribution characteristics of the scattering occurrence rate of the Jiamusi radar observation

Supporting Information:

Supporting Information may be found in the online version of this article.

Correspondence to:

J. Zhang and C. Wang, jjzhang@spaceweather.ac.cn; cw@spaceweather.ac.cn

Citation:

Wang, W., Zhang, J., Wang, C., Chen, J., Dang, T., Lei, J., & Ruohoniemi, J. M. (2023). Statistical characteristics of mid-latitude ionospheric F-region backscatter observed by the SuperDARN Jiamusi radar. *Radio Science*, 58, e2022RS007634. https://doi.org/10.1029/2022RS007634

Received 21 JAN 2023 Accepted 25 JUN 2023

Author Contributions:

Conceptualization: Jiaojiao Zhang
Data curation: Wei Wang, Junjie Chen
Formal analysis: Wei Wang, Jiaojiao Zhang
Methodology: Wei Wang, Jiaojiao Zhang
Project Administration: Jiaojiao Zhang
Resources: Chi Wang, Junjie Chen, Tong
Dang, Jiuhou Lei
Software: Wei Wang, Junjie Chen
Supervision: Jiaojiao Zhang, Chi Wang
Writing – original draft: Wei Wang
Writing – review & editing: Jiaojiao
Zhang, John Michael Ruohoniemi

© 2023. American Geophysical Union. All Rights Reserved.

Statistical Characteristics of Mid-Latitude Ionospheric F-Region Backscatter Observed by the SuperDARN Jiamusi Radar

Wei Wang^{1,2}, Jiaojiao Zhang^{1,2}, Chi Wang^{1,2}, Junjie Chen³, Tong Dang⁴, Jiuhou Lei⁴, and John Michael Ruohoniemi⁵

¹University of the Chinese Academy of Sciences, Beijing, China, ²State Key Laboratory of Space Weather, National Space Science Center (NSSC), Chinese Academy of Sciences, Beijing, China, ³Department of Earth Sciences, University of Hong Kong, Pokfulam, China, ⁴CAS Key Laboratory of Geospace Environment, School of Earth and Space Sciences, University of Science and Technology of China, Hefei, China, ⁵Department of Electrical and Computer Engineering, Virginia Polytechnic Institute and State University, Blacksburg, VA, USA

Abstract The Jiamusi (JME) radar is the first high-frequency coherent scatter radar independently developed in China. In this study, we investigate the statistical characteristics of the Jiamusi radar scattering occurrence rate from the F-region ionosphere between 40° N and 65° N geomagnetic latitude (MLAT) from March 2018 to November 2019. Then, the diurnal and seasonal variations in scattering echoes and their dependence on geomagnetic conditions are statistically investigated. It is shown that the local time of the peak scattering occurrence rate varies depending on the seasons, that is, approximately 20–22.5 magnetic local time (MLT) in summer, 17.5–20.5 MLT in equinox, and 16–17.5 MLT in winter, which is closely associated with the time of sunset. The occurrence rate also increases with the enhancement of the Kp index. To further understand the mechanism of these features, we simulate the distribution of the gradient drift instability (GDI) indicator $\nabla n \cdot \vec{V}/n$ by using the Thermosphere-Ionosphere-Electrodynamics General Circulation Model (TIEGCM). The analysis results indicate that the GDI may be one of the factors that contribute to these characteristic features.

1. Introduction

The Super Dual Auroral Radar Network (SuperDARN) initially consists of several high-frequency coherent radars in the Northern and Southern Hemispheres. The concept was developed to observe ionospheric convection's characteristics by detecting decameter-scale field-aligned irregularities (FAIs) in the polar region (Greenwald et al., 1995). In studies of irregularity convection in high latitudes using the SuperDARN radar data, it is found that during storm time, the convection pattern expands to the mid-latitudes and may eventually extend beyond the field of view of these radars. Then, the SuperDARN has included more mid-latitude radars to improve large-scale observations of ionospheric irregularities, and has currently more than 30 radars globally (Chisham et al., 2007; Greenwald et al., 1995; Nishitani et al., 2019). The eleventh (the newest) SuperDARN mid-latitude radar in the Northern Hemisphere was constructed in Jiamusi (46.8°N, 130.5°E, in geographic coordinates), China.

As the waves traverse the E and F regions of the ionosphere, if the direction of the wave vector is perpendicular to the direction of the magnetic field line when the signal encounters decameter-scale FAIs, they are scattered backward. The scattering occurrence rate depends on both the existence of FAIs and the conditions of high frequency (HF) wave propagation. Hence the observed scattering occurrence rate is considered to be a lower bound on the actual occurrence rate of FAIs, which provides essential information about the distribution of FAIs and their generation mechanism.

Over the past years, SuperDARN radars data have been used to make statistical studies of ionospheric scattering occurrence rates in the polar, auroral, and subauroral regions. The statistical characteristics of radar data in different latitudes are different. Using the SuperDARN Zhongshan radar (ZHO) data, statistical results showed that the high latitude ionospheric scattering occurrence rate was generally larger in winter than in summer (Hu et al., 2014). They also found that during geomagnetic quiet times, the peak scattering occurrence rate appears on the day side, shifts toward the night side, and exhibits a noticeable decrease with increasing Kp index. Hosokawa et al. (2001) first presented the statistical distributions of HF echoes in the subauroral region observed by six Northern Hemisphere SuperDARN radars. They found that the most prominent backscatter target of the

WANG ET AL. 1 of 10

Radio Science 10.1029/2022RS007634



SuperDARN radars is the scatter enhancement on the dusk side and thought that it corresponded to a plasma density depleted region, the mid-latitude trough. They also found that this feature is most clearly observed around the summer and winter solstices.

The studies on the scattering occurrence rate of mid-latitude SuperDARN radars show that their distribution characteristics are different from that of high-latitude radars, and the value is lower than that of high-latitude radar. A subsequent study by Hosokawa and Nishitani (2010) provided the results of the scattering occurrence rate of the Hokkaido East radar (HOK, located in 37.3°N and 144.9°W in geomagnetic coordinate) and the King Salmon radar (KSR, 57.5°N and 99.1°W in geomagnetic coordinate) and found that the scattering occurrence rate of lower latitude radar is lower than that of higher latitude radar. The results also showed that the enhancement of the scattering occurrence rate in the dusk side mainly occurs in the range of 59°–68° magnetic latitudes (MLAT). They thought the sunward plasma density gradient at the sunward edge of the mid-latitude trough and an ambient poleward electric field are the dominant drivers of the dusk side scatter occurrence rate enhancement.

The location of the JME radar is approximately 10° lower than the mid-latitude SuperDARN radars in North America, and a few degrees northward of the SuperDARN radars in Japan. It can observe the region from 40°N to 65°N MLAT. In this region, the distribution of scattering occurrence rates from high-frequency coherent scattering radars and their comparison with previous SuperDARN radar statistics will benefit the further understanding of mid-latitude ionospheric irregularities.

These decameter-scale FAIs may be driven by various instabilities resulting from the plasma drifts, density and temperature gradients, and electric fields (Fejer & Kelley, 1980; Keskinen & Ossakow, 1983; Tsunoda, 1988). The gradient drift instability (GDI) is an interchange instability that occurs in many regions in the ionosphere (Makarevich, 2014; Ossakow et al., 1978). The difference in the effect of ion-neutral and electron-neutral collisions causes a charge separation that leads to the creation of density irregularities in some time. In the ionospheric F region, the GDI can be stabilized when the ambient electric field, which generates the instability, has a modest component along the density gradient (Makarevich, 2014). At present, research showed that the scattering occurrence rate distribution in the dusk side and dawn side ionospheric F region may be related to the electronic density gradient, plasma drift velocity, and ionospheric electric field at the boundaries of the mid-latitude ionospheric trough (MIT) (Hosokawa et al., 2001). However, the distribution characteristics of the GDI at different magnetic local times and MLAT are still unclear, and the correlation between the GDI and the scattering occurrence rate enhancement in the F region of the mid-latitude ionosphere needs further study.

In this paper, we investigate the essential statistical characteristics of scattering occurrence rate in the F region by using observation data from the Jiamusi radar. We studied the diurnal and seasonal variations in the ionospheric scattering occurrence rate and their dependence on geomagnetic conditions (Kp index). For analyzing the GDI's mid-latitude distribution and its connection to radar statistics, the total electron content (TEC) data and the simulation results from Thermosphere-Ionosphere-Electrodynamics General Circulation Model (TIEGCM) are used to calculate the gradient density instability indicator ($\nabla n \cdot \nabla / n$) in this paper.

We briefly introduce the Jiamusi radar, the sources of the statistical data set, the data processing method, the TEC data, and the TIEGCM model in Section 2. The third section shows ionospheric scattering occurrence rate distributions under different seasonal and geomagnetic conditions. In the fourth section, we analyze the characteristics of these statistical results and combine them with the gradient density instability indicator. A discussion and summary are presented in Sections 5 and 6, respectively.

2. Data and Methods

2.1. Jiamusi Radar

Figure 1 shows the fields of view of the SuperDARN radars in the Northern Hemisphere. The fields of view of polar radars are marked in green, the rest of the high-latitude radars are marked in blue, and the mid-latitude radars are uniformly marked in red. A thick black line denotes the field of view of the Jiamusi radar. It is located at 46.8°N, 130.5°E in geographic coordinate (41.8°N, 155.1°W in altitude-adjusted corrected geomagnetic (AACGM) coordinate) and has been established and in operation since 2018. This radar comprises the main array of 16 twin-terminated folded dipole antennas. It operates in the frequency band from 8 to 20 MHz with both transmitting and receiving capabilities and has a four antennas interferometer array 100 m apart from the

WANG ET AL. 2 of 10

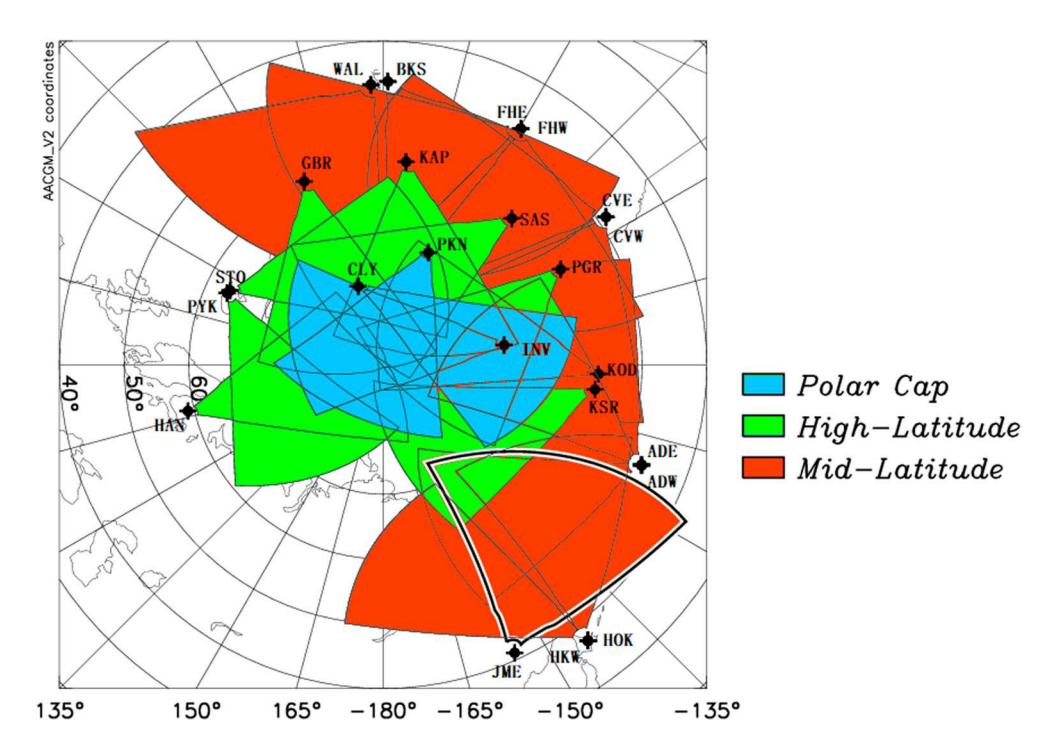


Figure 1. The fields of view of the Super Dual Auroral Radar Network radars in the Northern Hemisphere. Thick black lines indicate the field of view of the Jiamusi radar.

main array. The antennas can receive HF backscatter echoes from a slant range of 180–3,000 km and different ionospheric regions, depending on the number of gates (with a range resolution of 45 km). The boresight of the Jiamusi radar points 44° apart from the geographic north. Wang et al. (2022) and Zhang et al. (2020) validated the data by comparing the data from the Jiamusi radar and the Hokkaido East radar during disturbed and quiet geomagnetic conditions.

2.2. Data Set and Analysis

Parkinson et al. (2003) define the scattering occurrence rate as the total number of echoes during 15 min intervals at each of the 75 ranges per beam, divided by the total number of soundings made for a particular category of season and Kp. In our research, we use almost the same calculation as Parkinson, but the grid for calculating the occurrence rate was set as 12 min intervals at 1° interval of geomagnetic latitude.

Based on the characteristics of the echoes received by SuperDARN radars (both ground and ionospheric), several factors are considered for screening the ionospheric F region echoes. For example, the echo signal from the E region can be filtered through different distances, and the ground echo can be screened through an empirical formula related to Doppler velocity, Doppler spectral width, and signal-to-noise ratio.

Previous studies have suggested that in the SuperDARN radar observations, the radar echo whose distance is less than 600 km is regarded as backscatter from E region scatter. In comparison, echoes returned from a distance larger than 900 km are considered due to F region scatter (Ruohoniemi et al., 1988). Later, some researchers used 600 km as the dividing line of irregularity signals in the ionospheric F and E regions using the SuperDARN radar data (Parkinson et al., 2003). In this study, it is appropriate to use data with a gate larger than 14 (>630 km) for statistical analyses of ionospheric F-region scattering occurrence rate.

The empirical screening formula has been used to obtain scatter signals in HF coherent scattering radar echoes: $|V| - [V_{\text{max}} - (V_{\text{max}}/W_{\text{max}}) * |W|] > 0$ (Ribeiro et al., 2011), where W is the Doppler spectrum width, and V is the Doppler line of sight velocity, and in the current version of SuperDARN software, V_{max} is set to 30 m/s, and W_{max} is set to 90 m/s. At the same time, the ionospheric data set is also screened by excluding echoes with a low signal-to-noise ratio (SNR <3 dB), which can eliminate much of the ghost scatter due to radio interference (Parkinson et al., 2003).

WANG ET AL. 3 of 10

1944799x, 2023, 7, Downloaded

ibrary.wiley.com/doi/10.1029/2022RS007634 by Virginia Tech, Wiley Online Library on [13/07/2024]. See



Table 1Jiamusi Radar Data Under Different Conditions

Transfer Transfer Date: Different Containents				
	Summer(hr)	Equinox (hr)	Winter (hr)	Total (hr)
Kp < 2	2,061	1,773	1,188	5,022
$2 \le Kp < 3$	414	519	363	1,296
$Kp \ge 3$	237	324	177	738
Total	2,712	2,616	1,728	7,056

The statistical calculation uses data between March 2018 and November 2019. The number of hours of the measurements is shown in Table 1 and displays the time of valid data under different seasons and Kp conditions separately. The difference in the time of available data in each season is related to radar commissioning or maintenance.

2.3. Total Electron Content

The TEC is the total number of electrons present a path between a radio transmitter and receiver, measured in electrons per square meter. By convention, 1 TEC Unit (TECU) = 10^{16} electrons/m². This TEC data came from the Global

Navigation Satellite System (GNSS). The original configuration is set to be a $1^{\circ} \times 1^{\circ}$ geographic latitude-longitude grid, and the time step is 5 min. The data coordinate system is transformed from a geographic coordinate system to a geomagnetic coordinate system, and the average value of the data in each latitude grid in unit time was calculated. Finally, the TEC distribution results under AACGM coordinates are obtained.

2.4. TIEGCM

The TIEGCM is a comprehensive, first-principles, three-dimensional, nonlinear representation of the coupled thermosphere and ionosphere system. It included the dynamics, energetics, and chemistry with a steady-state ionospheric electrodynamo in a realistic geomagnetic main field defined by the International Geomagnetic Reference Field, developed by Dickinson et al. (1984), Richmond et al. (1992), and Roble et al. (1977). It has 29 constant-pressure levels in the vertical coordinates, extending from approximately 97–500 km in intervals of one-half scale height.

In the TIEGCM, the solar soft X-ray (XUV, 0–10 nm), extreme ultraviolet (EUV, 10–120 nm), and far ultraviolet (FUV, 120–200 nm) spectral fluxes are defined by the EUVAC model, using the observed F10.7 index. The model can obtain the distribution of ionospheric parameters at different altitudes. The simulation results of the ionosphere at 300 km altitude are presented in the following. The high latitude energy input associated with auroral particle precipitation is calculated by an analytical auroral model. The empirical Weimer (2005) model prescribes the electric potential at high latitudes. To merge the region of the wind dynamo with the high latitude region, a crossover boundary is introduced that varies dynamically with the strength of the magnetospheric forcing.

In our study, the grid spacing is 2.5° longitude and 2.5° latitude, and the time step is 10 min. At the same time, our inputs used the average of 10.7 cm solar radio flux of 2018 (F10.7 = 70) and the ideal geomagnetic index (Kp = 0, 2, and 4).

3. Statistical Results

Figure 2 shows the scattering occurrence rate sorted by different seasons (summer, equinox, and winter from left to right) when Kp < 2, which are color-coded according to the color bar shown on the right. The two green lines offer the distribution range of the 90-degree solar zenith angle (SZA) line each season. The marks 0, 6, 12, and 18 in the figure represent MLT. The data were collected on a grid of 12 min \times 1° MLAT.

Several regions of enhanced scattering occurrence rate exist in these figures. The peak rate (6%) occurs near sunset, with a slightly weaker rate at night (3%–4%) and a relatively weak rate near the dawn side and noon, except in winter. The enhanced occurrence rates at duskside appeared in 20–22.5 MLT in summer, 17.5–20.5 MLT in equinox, and approximately 16–17.5 MLT in winter. In winter, the enhancements of the scattering occurrence rate overlap with the distribution of the SZA 90° line, while in summer and equinox, the peak value of the rate appeared slightly later than the time of the SZA 90° line. The statistical results from Ruohoniemi et al. (1988) used the data from the Goose Bay radar and also showed that many echoes scatter events occurred when the SZA was larger than 95°. The peak scattering occurrence rate is approximately 5%–7%, lower than the 10% derived by Hosokawa et al. (2001).

Figure 3 shows the occurrence of ionospheric echoes in winter under different geomagnetic conditions. When the Kp index is less than 2, it is considered to be in a geomagnetic quiet period (left panel). When the $2 \le KP < 3$,

WANG ET AL. 4 of 10

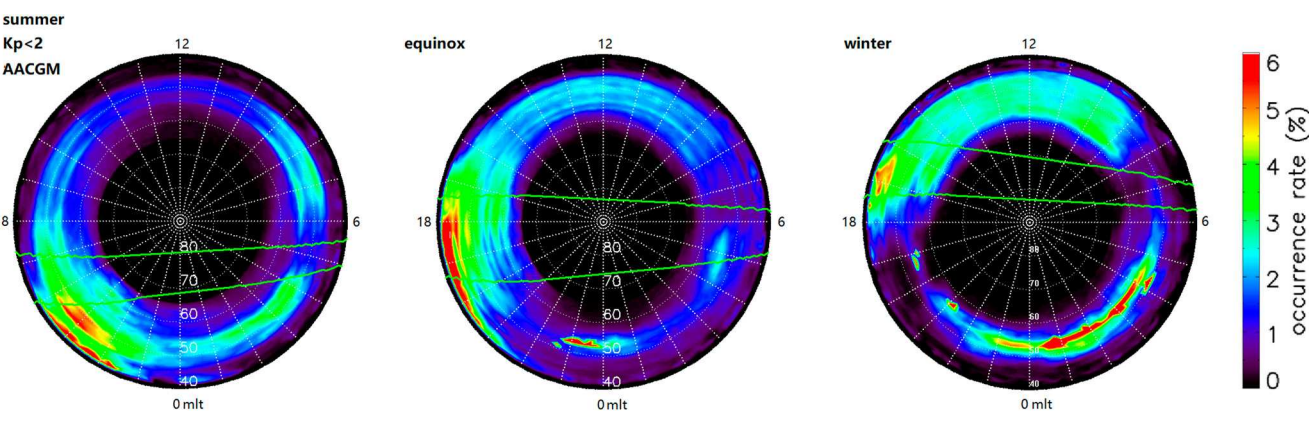


Figure 2. Distribution of the scattering occurrence rate during summer, equinox, and winter (from left to right) when Kp < 2. The results are shown in altitude-adjusted corrected geomagnetic coordinates, with noon at the top and dawn at the right. The green lines offer the distribution range of the solar zenith angle 90° line in the corresponding season.

(middle panel), it is considered to be in a weak disturbed period; when the index is greater than 3 (right panel), it is considered to be in a strong disturbance.

The most noticeable feature is that in the high geomagnetic active period, the occurrence rate of echoes is significantly higher than that in the quiet period. According to Jiamusi radar observation data, the range of occurrence rates greater than 6% increases as the geomagnetic index increases. Under all conditions, the occurrence rate was always relatively high on the dusk and night sides, similar to previous studies by Hosokawa and Nishitani (2010) and Ruohoniemi et al. (1988).

The interesting finding is that there is a long and narrow area with an increasing scattering occurrence rate at night in the mid-latitudes, which has received little attention in previous studies using the SuperDARN radar data. On the day side and dusk side, the enhanced scattering occurrence rate was present in the range of 40° – 65° MLAT, while on the night side, the improved scattering occurrence rate group was present in the field of 45° – 55° MLAT. There are seasonal variations in the time duration of the night side enhanced occurrence rate, which is related to the time of sunset.

4. Analysis

Hosokawa et al. (2001) proposed three different interpretation models for studying dusk scatter events using data from six Northern Hemisphere SuperDARN radars. They thought that the sunward plasma density gradient at the sunward edge of the mid-latitude trough (MIT) and an ambient electric field is a better mechanism for explaining the formation of FAIs. Using the Hokkaido East radar observation data from April 2007, Hosokawa and Nishitani (2010) calculated the echo occurrence rate in the subauroral region. The monthly average MLT-MLAT

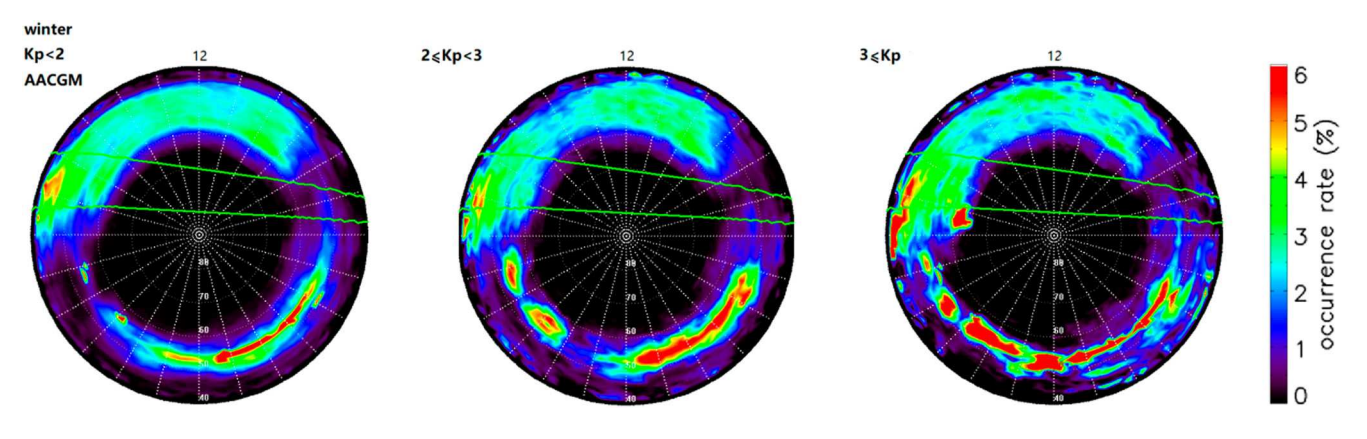


Figure 3. Distribution of the scattering occurrence rate in winter during different geomagnetic activities. From left to right are Kp < 2, $2 \le KP < 3$, and $Kp \ge 3$.

WANG ET AL. 5 of 10

distributions of the scattering occurrence rate in the F region observed by the Hokkaido East radar and the empirical formula for the location of the MIT are provided. They thought that the enhancement of the dusk side occurrence rate is closely related to the sunward edge of the MIT. Liu et al. (2021) studied the formation mechanism of F-region irregularities in the mid-latitude trough using data from Swarm in situ plasma measurements. They thought that the temperature GDI was the mechanism for plasma formation in the MIT at night.

This section will analyze the correlation between GDI and the scattering occurrence rate. In the F region, a general expression for the GDI growth rate is given by Makarevich (2014):

$$\gamma^{F} \cong \frac{GV_{E}}{1 + \Psi} \left(\vec{k} \cdot \vec{b} \times \vec{g} \right) \left(\vec{k} \cdot \vec{e} \right)$$
 (1)

where the gradient values $G = \nabla n/n$ (the n means the electron density). The V_E is the plasma drift velocity, the \vec{k} is the unit vector of the irregularity wave, the \vec{b} is the unit vector of the magnetic field, the \vec{g} is the unit vector of the density gradient, the \vec{e} is the unit vector of the electric field, and the ψ is the anisotropy factor which is much less than 1 in the F region ($\psi << 1$). The GDI growth rate is maximized along the bisector between the electric field and the cross-product of the gradient vector and magnetic field. In this paper, we calculate the GDI indicator $(\nabla n \cdot V/n)$ using electron density and plasma drift velocity simulated by the TIEGCM model and this indicator's distribution characteristics to analyze the Jiamusi radar irregularities occurrence rate in the mid-latitude F region.

Figure 4 shows the seasonal distributions when Kp = 0 (from left to right are summer, equinox, and winter) of the TEC observed by GNSS (top), plasma drift velocity simulated by TIEGCM (middle), and the GDI indicator (bottom). When the value is positive, GDI promotes the generation of irregularities; otherwise, it inhibits the generation. In the simulation, the summer solstice, autumn equinox, and winter solstice in 2018 were used to represent the plasma drift velocity distribution in summer, equinox, and winter.

In the top row of Figure 4, there is always a strong electron density gradient around sunset and sunrise. At sunset, the electron density gradient points southwest, and at sunrise, it means east or southeast. Around midnight and noon, there is a gradient of electron density toward the equator. The plasma drift velocity is mainly dominated by the west-direction velocity, with a weak north-south component. The GDI indicator is generally positive on the dusk side and negative on the dawn side, except in winter, which has a positive value on the dawn side. The distribution of its peak value also has seasonal variation, appearing at 19–23 MLT in summer, 17.5–22.5 MLT in equinox, and 16–20.5 MLT in winter.

Figure 5 shows (from top to bottom) the TECU, plasma drift velocity simulated by TIEGCM, and the GDI indicator in winter (the colorbar used in plasma drift velocity and GDI indicator is different). From left to right, the results are under the Kp = 0, Kp = 2, and Kp = 4 conditions. Since the seasonal variation trend under different geomagnetic conditions is similar, we show the distribution of various parameters in winter as a representative. When the Kp index is 4, the plasma density near noon is obviously enhanced, and the mid-latitude trough position moves slightly toward the equator at night. With the increase in geomagnetic activity, the simulation results of the GDI indicator also increase.

At sunset, the theoretical peak in the GDI indicator is consistent with the observed irregularity distribution. At sunrise, the GDI indicator is relatively small and even has a negative value, which may inhibit the emergence of irregularities. At night, a region with negative GDI parameters appeared at around 60° MLAT, and an extended narrow region with positive GDI parameters appeared south of 60° MLAT. This result is also similar to the characteristics of the observation data, and the GDI may affect the enhancement of the scattering occurrence rate at mid-latitude at night.

5. Discussion

In the results, at sunset and sunrise, the MLT distribution of the electron density gradient and the vector product of the electron density gradient and the plasma drift velocity have apparent seasonal variation. This characteristic is consistent with the echo occurrence rate variation in Figure 2. The increased scattering occurrence rate in the F region between 50° MLAT and 60° MLAT at nighttime is similar to the distribution characteristics of GDI parameters, which indicates that the variation in the GDI may be a factor affecting the seasonal variations in the occurrence rate of radar echoes.

WANG ET AL. 6 of 10

1944/799x, 2023, 7, Downloaded from https://agupubs.onlinelibrary.wiley.com/doi/10.1029/2022RS007634 by Virginia Tech, Wiley Online Library on [13/07/2024]. See the Terms and Conditions (https://onlinelibrary.wiley.com/erms-

and-conditions) on Wiley Online Library for rules of use; OA articles

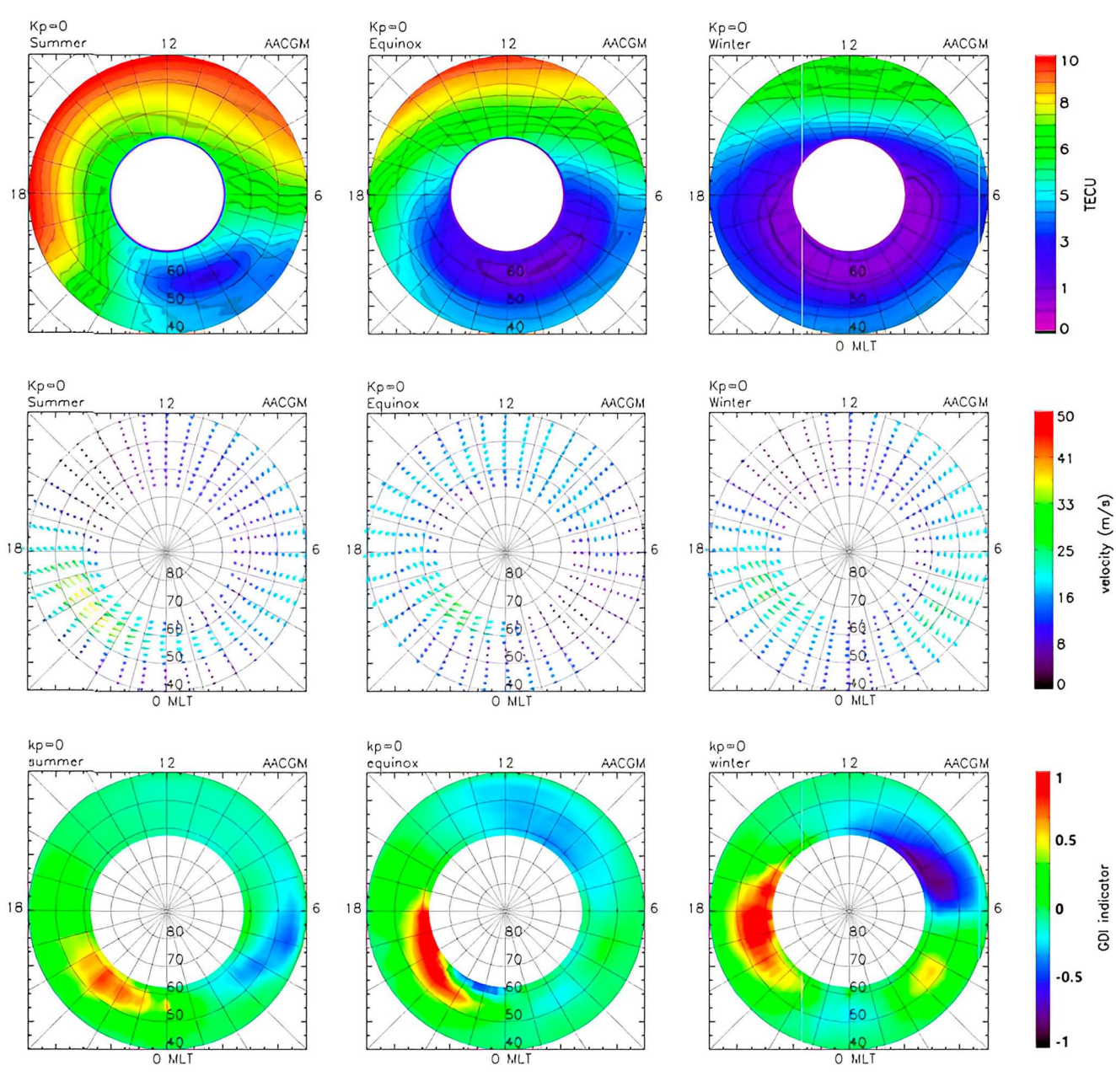


Figure 4. (Top row) Distribution of total electron content (TEC) when Kp = 0 during summer, equinox, and winter (from left to right). The plasma drift velocity (middle row) distribution in the Northern Hemisphere at the height of 300 km was obtained by the Thermosphere-Ionosphere-Electrodynamics General Circulation Model. The distribution of the gradient drift instability (GDI) indicator in different seasons (bottom row).

In addition to GDI instability, the night-side occurrence rate may be influenced by other factors. High-latitude convective electric fields can penetrate to the middle latitudes and affect the occurrence rate (Senior & Blanc, 1984), which is affected by various factors, such as geomagnetic activity, interplanetary magnetic field conditions, and ionospheric conductivity. Density fluctuations are amplified in plasma instability processes such as current-convective instability and temperature gradient instability (Liu et al., 2021). Current-convective instability occurs in regions where the field-aligned currents exceed a certain threshold, determined by the ambient parameters, and is often employed to explain the generation mechanism of FAIs associated with particle precipitation and field-aligned currents. This statistical result revealed that the night-side MIT region irregularities are strongly related to temperature GDI (mainly from 22 to 06 MLT).

WANG ET AL. 7 of 10

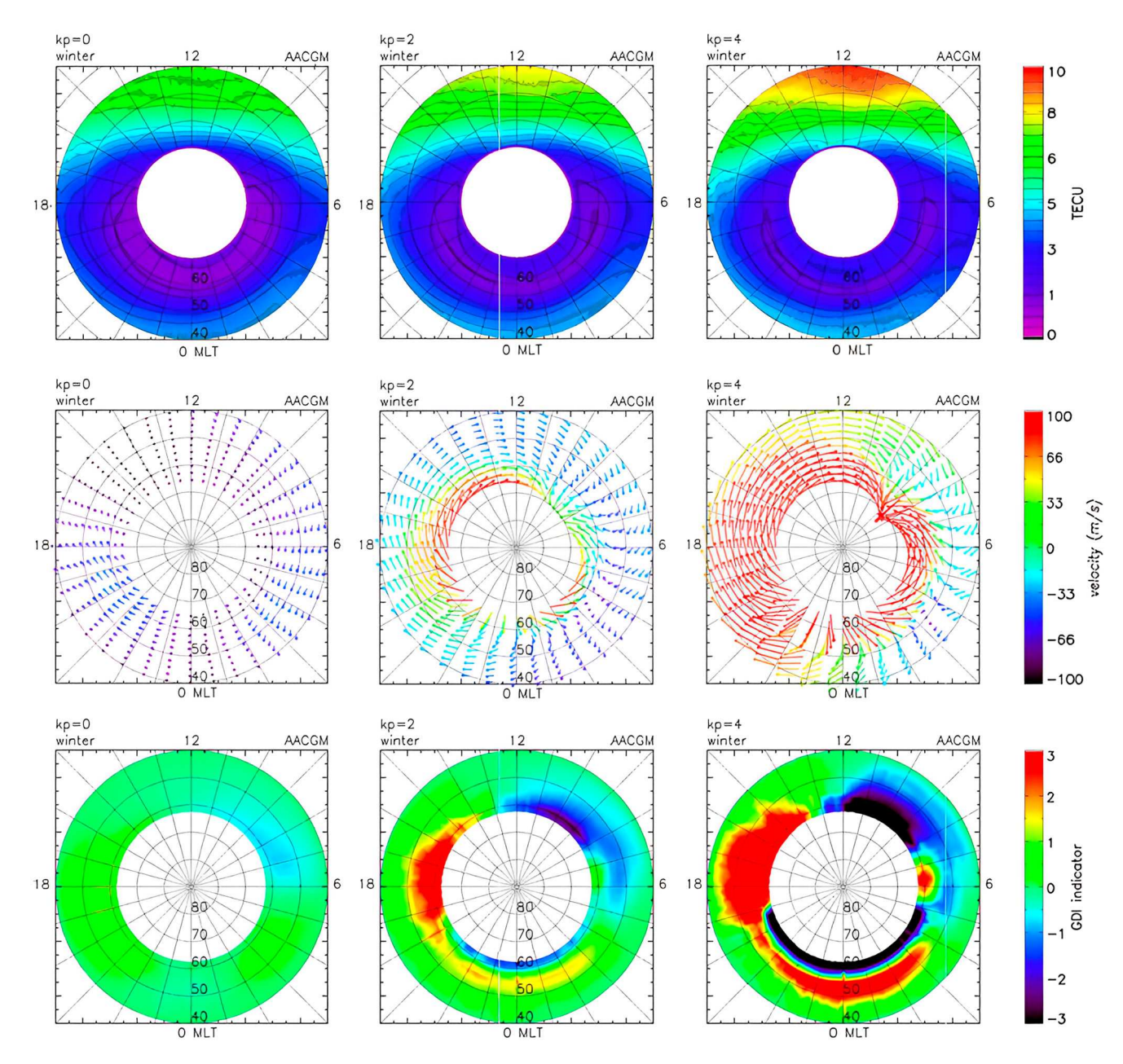


Figure 5. (Top row) Distribution of total electron content (TEC) in winter during different geomagnetic activities (from left to right are Kp = 0, 2, and 4). The plasma drift velocity (middle row) distribution in the Northern Hemisphere at the height of 300 km was obtained by the Thermosphere-Ionosphere-Electrodynamics General Circulation Model (winter solstice). The distribution of the gradient drift instability (GDI) indicator during different geomagnetic activities (bottom raw).

6. Summary

We investigated the mid-latitude ionospheric scattering occurrence rate using the SuperDARN Jiamusi radar. The statistical study examined the seasonal and diurnal variations of scattering echoes and their dependence on geomagnetic activity. The findings from this analysis are as follows:

- The Jiamusi radar ionospheric scattering occurrence rate depends on the MLT. The echo rate on the dusk side is successively stronger than on the night and day sides, and the occurrence rate on the dawn side is the weakest.
- 2. In different seasons, the maximum and minimum values of the ionospheric scattering occurrence rate always correspond to the location of the SZA 90° line. This phenomenon is consistent with the distribution of the GDI at that time.

WANG ET AL. 8 of 10

1944799x, 2023, 7, Downloaded from https

.com/doi/10.1029/2022RS007634 by Virginia Tech, Wiley Online Library on [13/07/2024]. See

3. There is a long and narrow area of enhanced scattering occurrence rate at night, similar to the nighttime distribution of GDI parameters.

This paper discusses the characteristics of the ionospheric scattering occurrence rate of the Jiamusi radar and its correlation with seasons and geomagnetic disturbance. It is considered that the SZA affects the distribution of the peak occurrence rate. The GDI is one of the factors for the scattering occurrence rate at sunset and sunrise between 40°N and 65°N MLAT. An accurate GDI distribution requires more HF radars to be built in the future to obtain a more accurate drift velocity.

Data Availability Statement

The full SuperDARN data set is published on the Federated Research Data Repository (FRDR) (https://www.frdr-dfdr.ca/repo/collection/superdarn). The Kp index is available from the World Data Center for Geomagnetism, Kyoto (http://wdc.kugi.kyoto-u.ac.jp/wdc/Sec3.html). The TEC data is available from the CEDAR Madrigal Database (http://cedar.openmadrigal.org/). To access the TEC data, users should enter user's name and email address to log in, choose "List experiments" in "Access data," select the instrument "Distributed Ground Based Satellite Receivers," then choose "World-wide GNSS Receivers Network." The TIEGCM code is available from the National Center for Atmospheric Research (NCAR) (https://www.hao.ucar.edu/modeling/tgcm/tie.php).

References

Chisham, G., Lester, M., Milan, S. E., Freeman, M. P., Bristow, W. A., Grocott, A., et al. (2007). A decade of the Super Dual Auroral Radar Network (SuperDARN): Scientific achievements, new techniques and future directions. Surveys in Geophysics, 28(1), 33–109. https://doi.org/10.1007/s10712-007-9017-8

Dickinson, R., Ridley, E., & Roble, R. (1984). Thermospheric general circulation with coupled dynamics and composition. *Journal of the Atmospheric Sciences*, 41(2), 205–219. https://doi.org/10.1175/1520-0469(1984)041<0205:TGCWCD>2.0.CO;2

Fejer, B. G., & Kelley, M. C. (1980). Ionospheric irregularities. *Reviews of Geophysics*, 18(2), 401–454. https://doi.org/10.1029/RG018i002p00401 Greenwald, R., Baker, K. B., Dudeney, J. R., Pinnock, M., Jones, T. B., Thomas, E. C., et al. (1995). DARN/SuperDARN - A global view of the dynamics of high-latitude convection. *Space Science Reviews*, 71(1–4), 761–796. https://doi.org/10.1007/BF00751350

Hosokawa, K., Iyemori, T., Yukimatu, A., & Sato, N. (2001). Source of field-aligned irregularities in the subauroral F region as observed by the SuperDARN radars. *Journal of Geophysical Research*, 106(A11), 24713–24732. https://doi.org/10.1029/2001JA900080

Hosokawa, K., & Nishitani, N. (2010). Plasma irregularities in the duskside subauroral ionosphere as observed with midlatitude SuperDARN radar in Hokkaido, Japan. *Radio Science*, 45(4), RS4003. https://doi.org/10.1029/2009RS004244

Hu, H.-Q., Liu, E., Liu, R., Yang, H., & Zhang, B.-C. (2014). Statistical characteristics of ionospheric backscatter observed by SuperDARN Zhongshan radar in Antarctica. Advances in Polar Science, 24(1), 19–31. https://doi.org/10.3724/SPJ.1085.2013.00019

Keskinen, M., & Ossakow, S. (1983). Nonlinear evolution of convecting plasma enhancements in the auroral ionosphere 2. Small scale irregularities. *Journal of Geophysical Research*, 88(A1), 474. https://doi.org/10.1029/JA088iA01p00474

Liu, Y., Xiong, C., Wan, X., Lai, Y., Wang, Y., Yu, X., & Ou, M. (2021). Instability mechanisms for the F-region plasma irregularities inside the midlatitude ionospheric trough: Swarm observations. *Space Weather*, 19(7), e2021SW002785. https://doi.org/10.1029/2021SW002785

Makarevich, R. (2014). Symmetry considerations in the two-fluid theory of the gradient drift instability in the lower ionosphere: MAKAREV-ICH. *Journal of Geophysical Research: Space Physics*, 119(9), 7902–7913. https://doi.org/10.1002/2014JA020292

Nishitani, N., Ruohoniemi, J. M., Lester, M., Baker, J. B. H., Koustov, A. V., Shepherd, S. G., et al. (2019). Review of the accomplishments of mid-latitude Super Dual Auroral Radar Network (SuperDARN) HF radars. *Progress in Earth and Planetary Science*, 6(1), 27. https://doi. org/10.1186/s40645-019-0270-5

Ossakow, S., Chaturvedi, P., & Workman, J. (1978). High altitude limit of the gradient drift instability. *Journal of Geophysical Research*, 83(A6), 30. https://doi.org/10.1029/JA083iA06p02691

Parkinson, M., Devlin, J., Ye, H. Y., Waters, C., Dyson, P., Breed, A., & Morris, R. (2003). On the occurrence and motion of decametre-scale irregularities in the sub-auroral, auroral, and polar cap ionosphere. *Annales Geophysicae*, 21(8), 1847–1868. https://doi.org/10.5194/angeo-21-1847-2003

Ribeiro, A., Ruohoniemi, J., Baker, J., Clausen, L., Larquier, S., & Greenwald, R. (2011). A new approach for identifying ionospheric backscatter in midlatitude SuperDARN HF radar observations. *Radio Science*, 46(4), RS4011. https://doi.org/10.1029/2011RS004676

Richmond, A., Ridley, E., & Roble, R. (1992). A thermosphere/ionosphere general circulation model with coupled electrodynamics. *Geophysical Research Letters*, 19(6), 601–604. https://doi.org/10.1029/92GL00401

Roble, R., Dickinson, R., & Ridley, E. (1977). Seasonal and solar cycle variations of the zonal mean circulation in the thermosphere. *Journal of Geophysical Research*, 82(35), 5493–5504. https://doi.org/10.1029/JA082i035p05493

Ruohoniemi, J., Greenwald, R., Villain, J. P., Baker, K., Newell, P., & Meng, C. I. (1988). Coherent HF radar backscatter from small-scale irregularities in the dusk sector of the subauroral ionosphere. *Journal of Geophysical Research*, 93(A11), 12871. https://doi.org/10.1029/JA093iA11p12871

Senior, C., & Blanc, M. (1984). On the control of magnetospheric convection by the spatial distribution of ionospheric conductivities. *Journal of Geophysical Research*, 89(A1), 261–284. https://doi.org/10.1029/JA089iA01p00261

Tsunoda, R. (1988). High-latitude F-region irregularities: A review and synthesis. Reviews of Geophysics, 26(4), 719–760. https://doi.org/10.1029/RG026i004p00719

Wang, W., Zhang, J., Wang, C., Nishitani, N., Yan, J., Lan, A., et al. (2022). Statistical characteristics of mid-latitude ionospheric irregularities at geomagnetic quiet time: Observations from the Jiamusi and Hokkaido East SuperDARN HF radars. *Journal of Geophysical Research: Space Physics*, 127(1), e2021JA029592. https://doi.org/10.1029/2021JA029502

Acknowledgments

This work was supported by National Key R&D Program of China 2022YFF0504400 and NNSFC Grants 42174210 and 42188101, and in part by the Specialized Research Fund for State Key Laboratories of China. We thank the National High-Tech Research and Development Program of China (863 program) for their support. The Jiamusi SuperDARN radar is maintained and operated by the National Space Science Center. We thank the Chinese Meridian Project for providing the Jiamusi radar data. We acknowledge the use of Super-DARN data. SuperDARN is a network of radars funded by national scientific funding agencies of Australia, Canada, China, France, Italy, Japan, Norway, South Africa, the United Kingdom, and the United States of America.

WANG ET AL. 9 of 10

Weimer, D. (2005). Improved ionospheric electrodynamic models and application to calculating Joule heating rates. *Journal of Geophysical Research*, 110(A5), A05306. https://doi.org/10.1029/2004JA010884

Zhang, J., Wang, W., Wang, C., Lan, A. L., Yan, J. Y., Xiang, D., et al. (2020). First observation of ionospheric convection from the Jiamusi HF radar during a strong geomagnetic storm. *Earth and Space Science*, 7(1), e2019EA000911. https://doi.org/10.1029/2019EA000911

WANG ET AL. 10 of 10